Hybridization-driven strong anharmonicity in Yb-filled skutterudites

Hong-Jie Pang,[1,2] Liu-Cheng Chen,[3,2] Hao Yu,[3,2] Peng-Fei Qiu,[4] Guo-Hua Zhong,[3,5] Qing Peng,[3] and Xiao-Jia Chen[2,3,*]

[1]*Key Laboratory of Artificial Structures and Quantum Control (Ministry of Education), School of Physics and Astronomy, Shanghai Jiao Tong University, Shanghai 200240, China*

[2]*Center for High Pressure Science and Technology Advanced Research, Shanghai 201203, China*

[3]*School of Science, Harbin Institute of Technology, Shenzhen 518055, China*

[4]*State Key Laboratory of High Performance Ceramics and Superfine Microstructure, Shanghai Institute of Ceramics, Chinese Academy of Sciences, Shanghai 200050, China*

[5]*Center for Photonics Information and Energy Materials, Shenzhen Institute of Advanced Technology, Chinese Academy of Sciences, Shenzhen 518055, China*

(Received 8 November 2021; revised 2 March 2022; accepted 17 March 2022; published 28 March 2022)

A high-pressure study of the structural and thermal transport properties is carried out on one of the most efficient filled skutterudites, $Yb_{0.3}Co_4Sb_{12}$, to understand the relatively low thermal conductivity behavior in this family. By combining x-ray diffraction and Raman scattering measurements, we detect a phase transition at around 12.4 GPa. The mode Grüneisen parameters of the observed phonon modes are obtained from the determined bulk modulus and the phonon frequency shifts with pressure. The strong anharmonicity in this material is demonstrated by the obtained large average Grüneisen parameter. We also find the depressed group velocity within the low-frequency range, the flat guest mode avoided crossing with the acoustic-phonon mode, and the significant contribution of optical phonons. The hybridization of the guest atom and host lattice and the related enhanced anharmonicity are suggested to account for the low lattice thermal conductivity in the studied system. These findings provide new insight into how phonon-phonon interactions lower lattice thermal conductivity in this important thermoelectric family.

DOI: 10.1103/PhysRevB.105.094115

I. INTRODUCTION

Thermoelectric materials are of great interest for sustainable energy applications due to their ability to convert waste heat into electricity. The high thermoelectric performance requires high power factor and low thermal conductivity. Finding materials with relatively low thermal conductivities or developing techniques to further lower the lattice thermal conductivities have been drawn a lot of attention in the past decades [1–4]. Filled skutterudite is one of the most prominent thermoelectric materials with a very low lattice thermal conductivity, as well as a large Seebeck coefficient and a good electrical conductivity [5]. Filling the parent skutterudites with guest atoms can significantly reduce the lattice thermal conductivity without deteriorating the electrical properties [6–9]. Much efforts have been concentrated on revealing the mechanism behind the low lattice thermal conductivity. The "phonon-glass-electron-crystal" concept has been employed to interpret the mechanism [10]. Within this picture, the guest atoms are loosely bound and act as "rattlers." These rattlers vibrate locally and incoherently, providing an additional phonon scattering channel to reduce the phonon mean free path. In such a way, the suppression of the thermal conductivity is attributed to the rattling of the guest atoms [11]. Meanwhile, a quasi-harmonic coupling between the guest atoms and the host lattice [12] was suggested from the neutron spectroscopy measurements along with the *ab initio* calculations on (La, Ce)Fe_4Sb_{12}. Interestingly, an independent vibration mode of Yb in $Yb_{0.2}Co_4Sb_{12}$ was observed by time-of-flight inelastic neutron scattering measurements (INS) [13]. The large effect of avoided crossing modes of Yb atoms to lowering the thermal conductivity has been reported in $YbFe_4Sb_{12}$ from first-principles calculations [14]. The avoided crossing between the acoustic modes and low-frequency optical modes has also been found in the phonon dispersion curve of $LaFe_4Sb_{12}$ through INS and density functional theory (DFT) calculations [15]. Additionally, the low lattice thermal conductivities in filled skutterudite compounds were also proposed to be related to the large anharmonicity [16,17]. Therefore no agreement has been reached on the mechanisms behind the low lattice thermal conductivity.

Phonon dispersion and lattice anharmonicity can provide crucial information to understand the lattice thermal conductivity. Phonon vibrational properties are usually studied by using INS, inelastic x-ray scattering, and Raman scattering techniques. For example, the neutron technique has been widely used to obtain the phonon density of states (DOS) in filled skutterudites [12,13,15,16,18]. The Raman technique has been proven to be powerful in providing equivalent phonon vibrational information with the others [19–21] but has many advantages such as high resolution and small sample size. It is a unique technique to detect the phonon vibrational information of thermoelectric materials at a wide temperature range [22,23] or at high pressures [24–26]. The effects of the lattice anharmonicity on the lattice thermal conductivity

*xjchen2@gmail.com

in thermoelectric materials through the experimentally determined mode Grüneisen parameters have been established from recent high-pressure studies [24–27]. The importance of the Raman scattering technique in providing phonon information has been emphasized recently on filled skutterudites [28–30]. Since the number of atoms in the primitive cell of filled skutterudites is relatively large, the assignments of the relevant phonon modes as well as the measurements down to the frequency as low as possible are not an easy task. Therefore the contribution of the optical modes to the lattice thermal conductivity in filled skutterudites needs to be examined in detail. Notably, Raman scattering is not sensitive to the filling atom because filling atom to the parent skutterudite adds an infrared-active mode. At present, the accurate mode Grüneisen parameters for filled skutterudites are not available yet. The effects of the anharmonicity on the lattice thermal conductivity wait for the evaluation. Therefore the efforts from both the experiments and calculations along this direction are highly desired.

In this work, we report x-ray diffraction (XRD) and Raman scattering measurements as well as first-principles calculations of phonons in a prominent filled skutterudite $Yb_{0.3}Co_4Sb_{12}$ at high pressures to settle down the issues mentioned above. The crystal structure and its evolution with pressure are determined by the XRD measurements with the help of the observed phonon modes obtained from Raman spectroscopy. The structural and phonon vibrational properties are further used to obtain the bulk modulus and mode Grüneisen parameters of the filled skutterudite. First-principles calculations are carried out to obtain the phonon dispersion and lattice thermal conductivity. The experiments and calculations provide a thoughtful understanding of the thermal transport properties in this filled skutterudite.

II. EXPERIMENTAL AND CALCULATION DETAILS

The sample was synthesized by a melt spinning and spark plasma sintering process. The detailed process can be found elsewhere [31]. The actual composition of the sample was determined by an energy dispersive spectrometer (EDS, OXFORD). The ambient-pressure structure of the sample was characterized using a RigakuD/MAX-2550PC diffractometer under Cu K_α radiation with a wavelength of 1.5406 Å.

For the high-pressure structural study, the *in situ* synchrotron XRD patterns were collected at the Advanced Phonon Source (APS), Argonne National Laboratory (ANL), the U.S.A. with a wavelength of 0.3344 Å and a focused beam of less than 2 micrometers. A symmetric diamond anvil cell (DAC) with a culet size of 300 μm in diameter was used to load the sample. The sample was ground into fine powder grains before being placed into the DAC. Neon was loaded as the pressure transmitting medium to generate the hydrostatic pressure environment. The pressure was calibrated by the ruby fluorescent shift method [32]. The raw images were integrated into XRD patterns using FIT2D software [33]. The intensity versus 2θ diffraction patterns were refined by the Rietveld method using GSAS software [34,35].

For the high-pressure Raman scattering measurements, the pressure was applied by the same DAC as that used in the high-pressure XRD measurements. The Raman spectra were collected with an excitation laser wavelength of 488 nm emitted by a sapphire laser (Coherent). The scattered light was focused on an 1800 g/mm grating and recorded by a Princeton Instrument spectrometer coupled to a Charge-Coupled-Device. The Raman notch filters have a very narrow bandpass, allowing the measurements of Raman spectroscopy to be as low as 10 cm^{-1}. The laser power was kept below 2.5 mW before a $\times 20$ objective to avoid possible damage to the sample. Neon was also loaded as the pressure transmitting medium. The pressure was measured by the ruby fluorescent method [32].

All the calculations were performed on the basis of DFT. Vienna *ab initio* simulation package (VASP) was used for these calculations [36,37]. The lattice constant, phonon dispersion, lattice thermal conductivity, group velocity, and anharmonic scattering rates were determined from the harmonic and the third-order interatomic force constants (IFCs). The projector augmented wave (PAW) method with a Perdew-Burke-Ernzerbof-type generalized gradient approximation (GGA) [38] was employed for the calculations. The plane-wave basis set with a cutoff energy of 520 eV was used for the valance electrons. The lattice constants and ionic coordinates were relaxed to find the most stable states for $CoSb_3$ and $YbCo_4Sb_{12}$. The geometry optimization of the unit cell was done with a $5 \times 5 \times 5$ k-point grid. The IFCs were calculated within real-space supercell approaches using the PHONOPY package [39] for the harmonic IFCs and the SHENGBTE package [40] for the third-order IFCs.

III. RESULTS AND DISCUSSION

A quantitative evaluation of the phonon-phonon anharmonic interactions requires the Grüneisen parameter. Generally, a large Grüneisen parameter indicates strong phonon-phonon anharmonic interactions that result in low lattice thermal conductivity. Here, we present a direct experimental measurement of the Grüneisen parameters for the phonon modes. The Grüneisen parameter (γ_i) describes the volume dependence of phonon frequency, defined as [41]

$$\gamma_i = -\frac{d\ln\omega_i}{d\ln V} = \frac{B_0}{\omega_i}\frac{d\omega_i}{dP}, \tag{1}$$

where V is unit-cell volume, B_0 is the bulk modulus at ambient pressure, ω_i is the frequency of the phonon mode, and P is pressure. By definition, measurement of the mode Grüneisen parameters requires bulk modulus and phonon mode shifts with pressure.

A. Structural evolution with pressure

First, we determine the structure of the sample at room temperature. The sample belongs to the $Im\bar{3}$ space group. The lattice parameter at ambient pressure [$a = 9.0623(7)$ Å] agrees well with the literature [31]. The *in situ* synchrotron XRD patterns at high pressure up to 52.2 GPa are shown in Fig. 1(a). All the diffraction peaks monotonically shift to higher angles with increasing pressure, indicating the shrinkage of the lattice. We observed no new peaks appear or no peaks merge

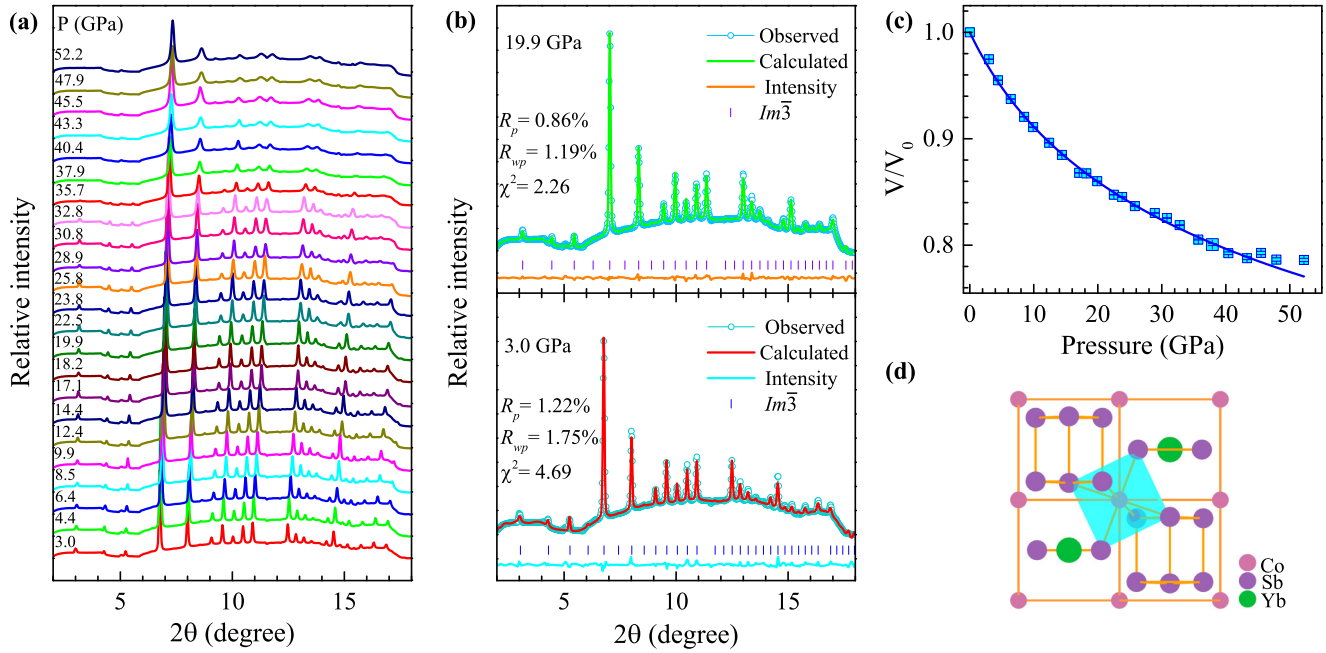

FIG. 1. (a) Synchrotron XRD patterns of $Yb_{0.3}Co_4Sb_{12}$ under pressure. The corresponding pressure is marked next to each curve. (b) The XRD patterns and Rietveld refinement results at representative pressures of 3.0 and 19.9 GPa. The experimental and fitted data points are plotted together by the open circles and thin curves. Vertical sticks represent reflection markers at the lower patterns. Thin curves at the bottom of each panel indicate the differences between the observed and calculated patterns. (c) Pressure dependence of the relative unit cell volume in $Yb_{0.3}Co_4Sb_{12}$. Solid lines represent the fitting of a BM-EOS to data. (d) The crystal structure of the $Im\bar{3}$ phase.

and/or split within the studied pressure range. Figure 1(b) shows the refined results at the selected pressures of 3.0 and 19.9 GPa using the Rietveld method. The structural models with the initial space group of $Im\bar{3}$ produce the experimental data very well. In the studied pressure range, no significant change in the XRD spectra indicating any deviation from cubic symmetry is observed. The calculated refinement factors are $R_p = 1.22\%$, $R_{wp} = 1.75\%$, and $\chi^2 = 4.69$ for 3.0 GPa and $R_p = 0.86\%$, $R_{wp} = 1.19\%$, and $\chi^2 = 2.26$ for 19.9 GPa, indicating reliable results. Figure 1(d) illustrates the crystal structure of the sample.

Investigating the mode Grüneisen parameter requires the bulk modulus. Figure 1(c) demonstrates the pressure dependence of relative unit cell volume. All data points have error bars smaller than the symbols. The relative volume monotonically decreases with increasing pressure. No anomaly is observed. The volume evolution with pressure can be described by the third-order Birch-Murnaghan equation of state (BM-EOS) [42]

$$P = \frac{3}{2}B_0\left[\left(\frac{V_0}{V}\right)^{\frac{7}{3}} - \left(\frac{V_0}{V}\right)^{\frac{5}{3}}\right] \times \left\{1 + \frac{3}{4}(B_0' - 4)\left[\left(\frac{V_0}{V}\right)^{\frac{2}{3}} - 1\right]\right\}, \quad (2)$$

where B_0' is the bulk modulus pressure derivative at ambient conditions. The fitting yields $B_0 = 75 \pm 2.81$ GPa with B_0' = 6.91 ± 0.32. The bulk modulus is smaller than that of unfilled skutterudite $CoSb_3$ [$B_0 = 93(6)$ GPa] at pressures below 20 GPa [43]. Like a previous study [44], the filled Yb atoms enlarge the cell parameter, and the expansion of the structure lowers the bulk modulus of filled skutterudite. Notably, the bulk modulus of the sample is also much smaller than those of other filled skutterudites, such as $LaFe_3CoSb_{12}$ [$B_0 = 87.4(6)$ GPa] [44], $CeFe_4Sb_{12}$ [$B_0 = 80(8)$ GPa] [45], $Ce_{0.8}Fe_3CoSb_{12}$ [$B_0 = 83(2)$ GPa] [45], and $Eu_{0.84}Fe_4Sb_{12}$ [$B_0 = 100(2)$ GPa] [46].

The bulk modulus obtained in $Yb_{0.3}Co_4Sb_{12}$ is similar to the behavior observed in unfilled skutterudite $CoSb_3$ [43]. In the case of $CoSb_3$, the fitting of the volume evolution with pressure to the whole data set has no volume discontinuity and yields a much smaller value [$B_0 = 50(16)$ GPa)] than the value below 20 GPa. This bulk modulus change has been interpreted as an irreversible isosymmetric phase transition, namely, the pressure-induced self-insertion reaction of Sb. According to the case in unfilled skutterudite $CoSb_3$ [43], we fitted the volume evolution with pressure up to 20 GPa in $Yb_{0.3}Co_4Sb_{12}$. The yielded bulk modulus [$B_0 = 84(5)$ GPa)] is larger than the value to the full pressure range and comparable to those of other filled skutterudites. In terms of $CoSb_3$, the difference in bulk modulus above 20 GPa is attributed to the self-insertion of Sb atoms [43]. For Yb-filled $CoSb_3$, a Yb atom occupying the 2*a* site could hinder the Sb atom from taking the position. The difference in bulk modulus around 12 GPa has been observed in $Eu_{0.84}Fe_4Sb_{12}$ [46]. A decoupling and subsequent reconstruction of the low-energy Eu mode and acoustic phonon modes have been suggested to be responsible for the change in the bulk modulus of $Eu_{0.84}Fe_4Sb_{12}$. Therefore the change of bulk modulus $Yb_{0.3}Co_4Sb_{12}$ may originate from lattice distortion, defects, or a decoupling and subsequent re-

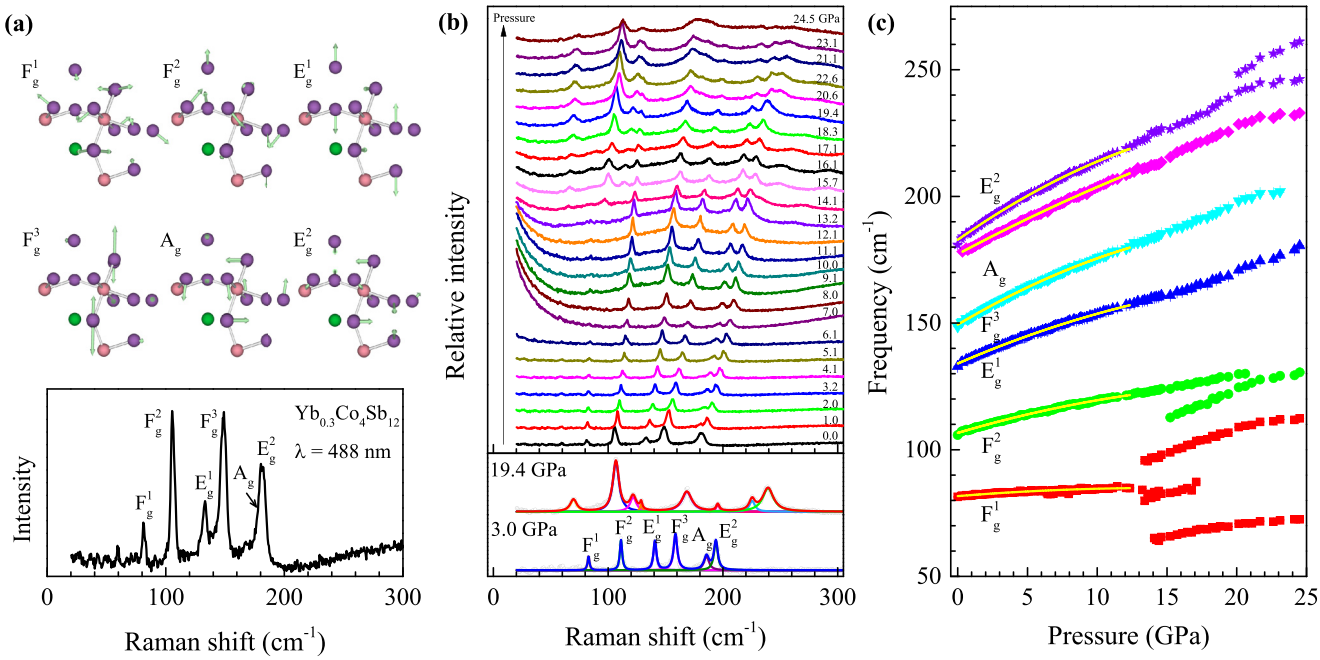

FIG. 2. (a) Raman spectra of $Yb_{0.3}Co_4Sb_{12}$ at ambient pressure and room temperature (bottom). The top panel shows the phonon modes' assignments. The arrows represent the vibrational directions of the atoms, pink for Co, purple for Sb, and green for Yb. (b) Evolution of Raman spectra in $Yb_{0.3}Co_4Sb_{12}$ with pressure at room temperature (top). The Raman spectra are plotted with open cycles and fitted by the Lorentz function. Representative Raman spectra at 3.0 and 19.4 GPa are shown in the lower panel. (c) Pressure-dependent frequencies of the phonon modes in $Yb_{0.3}Co_4Sb_{12}$. The solid lines are the quadratic fittings to the experimental data points.

construction of the low-energy Yb mode and acoustic phonon modes by pressure.

B. Evolution of vibrational properties with pressure

Raman scattering measurements are sensitive to subtle structural changes and facilitate the accurate detection of the crystal structure transitions through the probe of local vibrational modes. The investigation of the mode Grüneisen parameter also requires the Raman shift for each phonon mode. We collected the Raman spectra on $Yb_{0.3}Co_4Sb_{12}$ with a 488 nm excitation source and the resolution is better than 1 cm^{-1}, as shown in the lower panel of Fig. 2(a). According to group theory, 17 atoms in the primitive cell of $YbCo_4Sb_{12}$ give rise to 51 different vibrational modes, including three acoustic modes and 48 optical modes. Therefore the contribution of optical modes to the lattice thermal conductivity is obviously important. According to the irreducible representation, the optical phonon modes at the Γ point can be denoted as $\Gamma = 2A_g \oplus 2E_g \oplus 4F_g \oplus 2A_u \oplus 2E_u \oplus 8F_u$. The modes with A_g, E_g, and F_g symmetries are Raman active, and consequently, there are eight Raman-active modes [47]. In accordance with first-principles calculations, the observed six peaks in the lower panel of Fig. 2(a) are determined as $3F_g$, $1A_g$, and $2E_g$, respectively [11]. The phonon peaks of $Yb_{0.3}Co_4Sb_{12}$ are wider and the frequencies are lower than those of unfilled skutterudite $CoSb_3$ [47,48], which is consistent with the theoretical calculations [11]. The assignments of the corresponding phonon modes are demonstrated in the upper panel of Fig. 2(a). The arrows represent the vibrational directions of the atoms, pink for Co, purple for Sb, and green for Yb. All the observed modes are the motions of Sb. These results are in accordance with the contributions of the atoms to the vibrational density of states [11].

The evolution of the Raman spectra of $Yb_{0.3}Co_4Sb_{12}$ with pressure at room temperature is shown in the upper panel of Fig. 2(b). Most of the Raman peaks monotonically shift toward higher frequencies with increasing pressure. The sudden increase in Rayleigh intensities near 6 GPa is due to the solidification of the pressure transmitting medium. At higher pressures, some new peaks can be observed. This means that some changes may happen to the lattice structure. Considering that a new mode due to self-inserting Sb atoms would give an infrared-active Fu mode in the case of an ideal crystal [47], the origin of the new peaks in the Raman spectra may be due to the lattice distortion, defects, or a decoupling and subsequent reconstruction of the low-energy Yb mode and acoustic phonon modes by pressure [46]. The phonon frequency of each phonon mode is fitted by the Lorentz formula. According to the XRD data, the representative Raman spectra at pressure of 3.0 and 19.4 GPa are shown in the lower panel of Fig. 2(b). The pressure-induced changes can be observed from the two Raman spectra. Fitting the Raman spectra gives the extracted pressure-dependent frequencies of each phonon mode. Figure 2(c) demonstrates the pressure-dependent frequencies of the phonon modes in $Yb_{0.3}Co_4Sb_{12}$. Around 12.4 GPa, new peaks near the two F_g modes at low frequencies are observed.

Due to the sample's similar profiles and space groups, it is difficult to determine the structural phase transition from the XRD analysis. Raman scattering can detect small variations in structures that are invisible to XRD. The emergence of new

TABLE I. Summary of the vibrational mode, frequency ω_{i0} (cm^{-1}), pressure derivative $d\omega_i/dP$ (cm^{-1}/GPa), $d^2\omega_i/dP^2$ ($\times$ 10^{-2} cm^{-1}/GPa^2), and mode-Grüneisen parameter γ_i for each phonon mode of $Yb_{0.3}Co_4Sb_{12}$.

Mode	ω_{i0}	$d\omega_i/dP$	$d^2\omega_i/dP^2$	γ_i
F_g^1	81.68 ± 0.06	0.45 ± 0.03	-0.02 ± 0.00	0.50 ± 0.07
F_g^2	106.62 ± 0.05	1.64 ± 0.03	-0.03 ± 0.00	1.40 ± 0.12
E_g^1	134.02 ± 0.09	2.39 ± 0.03	-0.04 ± 0.00	1.62 ± 0.14
F_g^3	149.39 ± 0.06	3.27 ± 0.03	-0.07 ± 0.00	1.99 ± 0.16
A_g	177.07 ± 0.13	2.96 ± 0.04	-0.03 ± 0.0	1.52 ± 0.13
E_g^2	182.87 ± 0.12	3.86 ± 0.05	-0.07 ± 0.0	1.92 ± 0.16
			averaged γ_i	1.49 ± 0.13
$CoSb_3^{cal.}$				1.111 [49]
$CoSb_3^{exp.}$				0.952 [50]

peaks indicates a phase transition at high pressures. However, the current structural data are not enough to pin down the accurate lattice structure. Additionally, the sample demonstrates excellent thermoelectric performance in the first phase. Investigating the thermoelectric properties at ambient pressure is unaffected by the phase change. For those, we concentrate on the vibrational properties of the sample at pressures below 12.4 GPa. Refitting the volume evolution with pressure below 12.4 GPa yields the bulk modulus $B_0 = 91.01 \pm 6.72$ GPa with $B_0' = 3.46 \pm 1.56$. The former is slightly larger than those of other filled skutterudites [44–46].

In addition, the high-frequency phonon modes have more obvious shifts with increasing pressure, as shown in Fig. 2(c). The low-frequency phonon mode at about 80 cm^{-1} increases more gently. The difference suggests that the high-energy phonons are more sensitive to pressure than the low-energy phonons in the sample. The pressure dependence of the phonon frequencies at pressures below 12.4 GPa are fitted by a quadratic formula:

$$\omega_i(P) = \omega_{i0} + (d\omega_i/dP)P - (d^2\omega_i/dP^2)P^2, \qquad (3)$$

where ω_{i0} is the frequency of the phonon mode at ambient pressure and room temperature. The fitted results are summarized in Table I.

C. Evaluation of the phonon anharmonicity

We obtain the experimental Grüneisen parameters of each phonon mode by combining the bulk modulus and Raman shift of phonon modes. The obtained phonon frequencies, their pressure derivatives, and Grüneisen parameters for each phonon mode are listed in Table I. These results provide a new perspective on understanding the phonon anharmonicity in filled skutterudites. As mentioned above, a large Grüneisen parameter value means strong lattice anharmonicity. Thus, due to their relatively large values, the phonon mode F_g^3 at 149 cm^{-1} with $\gamma = 1.99$ and the phonon mode E_g^2 at 182 cm^{-1} with $\gamma = 1.92$ play prominent roles in the procedure of phonon scatterings. The mode Grüneisen parameters of $Yb_{0.3}Co_4Sb_{12}$ are close to those reported in $CoSb_3$ [47] and only slightly larger for $Yb_{0.3}Co_4Sb_{12}$. Notably, the low Grüneisen parameter value for the F_g^1 mode at about 82 cm^{-1} ($\gamma = 0.5$) is very close to the one predicted for $CoSb_3$ by DFT calculations ($\gamma = 0.3$) [47].

Additionally, we further calculated the average Grüneisen parameter of the six phonon modes based on $\bar{\gamma} = \sqrt{(\gamma_i^2)} = 1.49 \pm 0.13$. This is the first experimental data available for efficient filled skutterudites. It should directly measure the quantitative anharmonicity to investigate the low lattice thermal conductivity in filled skutterudites. The obtained bulk modulus and Raman shift of phonon modes are on the basis of the same sample in the same good pressure transmitting medium. Thus the determined mode Grüneisen parameters are reliable and should capture the nature of the phonon anharmonicity. Notably, we find that the obtained $\bar{\gamma}$ is larger than the values of unfilled skutterudite $CoSb_3$ [49,50]. This means that the strong anharmonicity contributes to the reduced lattice thermal conductivity in filled skutterudites.

D. Avoided crossing of the guest mode and acoustic-phonon branches

To gain a comprehensive understanding of the low lattice thermal conductivity, we performed the first-principles calculations on $YbCo_4Sb_{12}$. The phonon dispersions and DOS of $YbCo_4Sb_{12}$ are shown in Fig. 3. The data for $CoSb_3$ are given for comparison. All the phonon frequencies are positive and no imaginary frequencies are found, indicating that the structures are dynamically stable. In $YbCo_4Sb_{12}$, a large gap at about 200 cm^{-1} and a smaller gap at about 100 cm^{-1} are observed. The high-energy above 220 cm^{-1} and the low-energy below 200 cm^{-1} are mainly from the vibrations of the Co and Sb atoms, respectively. An additional triple-degenerate optical band at 42 cm^{-1} is added, which is not present in $CoSb_3$. This band is flat and close to the acoustic bands. By comparing the DOS of $YbCo_4Sb_{12}$ and $CoSb_3$, we attribute this band to a localized vibration of Yb.

The computed phonon dispersions and DOS are in good agreement with the experimental data and other calculations [9,13–16,51,52]. Note that the flat guest mode corresponds to the vibration mode of Yb at about 40 cm^{-1} in $Yb_{0.2}Co_4Sb_{12}$ by time-of-flight INS measurements and theoretical calculations [13]. A similar mode at the close frequency (46 cm^{-1}) has been observed by high-resolution INS and inelastic x-ray scattering measurements and *ab initio* powder-averaged lattice-dynamics calculations on $YbFe_4Sb_{12}$ [16]. However, the low-frequency of the Yb vibrational mode is significantly smaller than that of the La mode through three-axis inelastic neutron spectroscopy on $LaFe_4Sb_{12}$ (54 cm^{-1}) [15] and first-principles calculations on $La_{0.125}Co_4Sb_{12}$ (66 or 68 cm^{-1}) [9,52]. The difference may be attributed to the relatively large Yb mass compared with others.

The phonon modes between 80 cm^{-1} and 200 cm^{-1} are dominated by the vibrations of the Sb atoms. The phonon dispersions allow us to assign several Raman features observed for $Yb_{0.3}Co_4Sb_{12}$. The assignments agree with our results from Raman scattering measurements.

Compared with $CoSb_3$, the filling of the Yb guest atom significantly downshifts the vibrational modes, as shown in Figs. 3(a) and 3(c). This behavior is consistent with the Raman spectra of $Yb_{0.3}Co_4Sb_{12}$ (Fig. 2). Generally, phonon softening

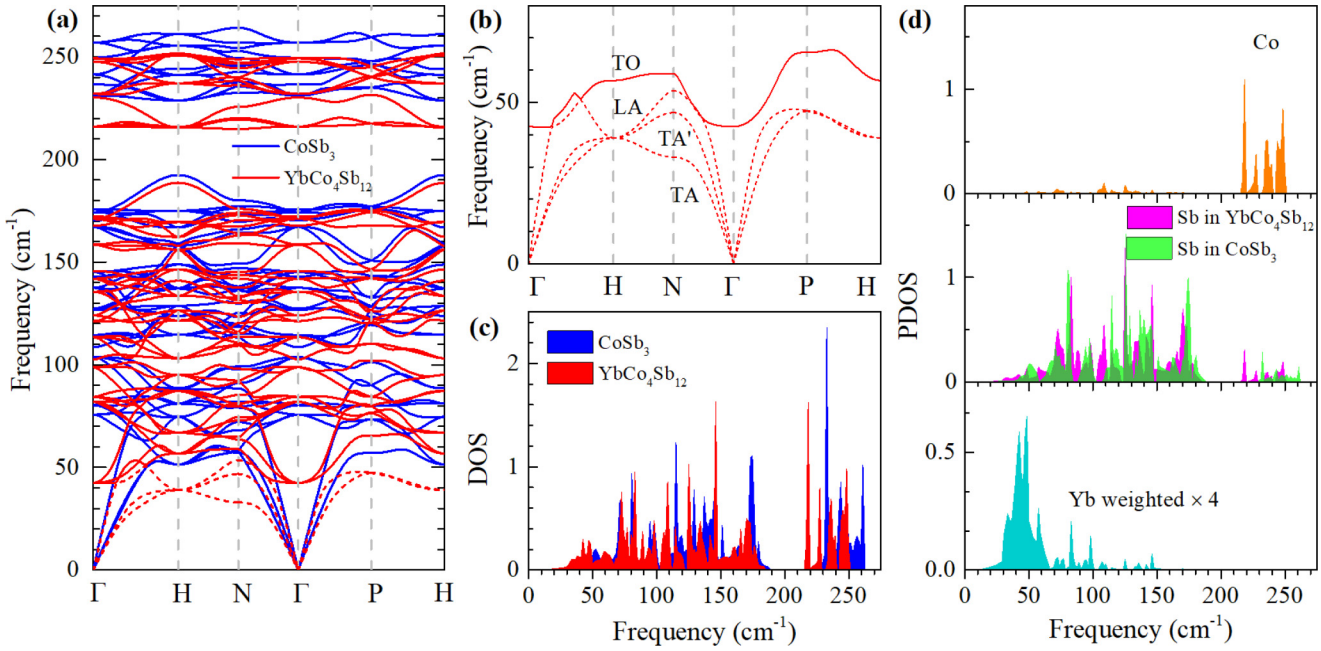

FIG. 3. (a) Phonon dispersions in $YbCo_4Sb_{12}$ and $CoSb_3$ from first-principles calculations. (b) Phonon dispersions of acoustic modes and Yb mode in $YbCo_4Sb_{12}$. (c) Calculated total density of states in $YbCo_4Sb_{12}$ and $CoSb_3$. (d) Calculated projected density of states in $YbCo_4Sb_{12}$. The dispersions of $CoSb_3$ and $YbCo_4Sb_{12}$ are represented by the blue and red lines, respectively. The acoustic branches of $YbCo_4Sb_{12}$ are represented by dashed red lines. The projected density of states of Co, Sb, and Yb in $YbCo_4Sb_{12}$ are labeled as orange, magenta, and cyan blocks, respectively. The projected density of states of Sb in $CoSb_3$ are labeled as green blocks.

is beneficial to yield low thermal conductivity. The acoustic bands are flatter in $YbCo_4Sb_{12}$. This means lower group velocities for acoustic bands due to the Yb guest atom. All of these contribute to the low lattice thermal conductivity.

An important finding from Fig. 3 is that the guest mode is flat and avoided crossing with the acoustic phonon mode. The details are given in Fig. 3(b). Phonon displacements in cubic crystals can be decomposed into one longitudinal branch and two transverse branches. The longitudinal branch is along the phonon propagation vector and the transverse branches are perpendicular to the propagation direction. Figure 3(b) clearly reveals that two transverse (TA) and a longitudinal (LA) acoustic modes propagate from the zone center and approach the zone boundary. A flat mode is observed at 42 cm^{-1} near the zone center. The avoided crossing of the LA mode mixing with the flat longitudinal guest mode (TO) is clearly observed. The avoided crossing found here is consistent with the INS results on $YbFe_4Sb_{12}$ and $LaFe_4Sb_4$ and DFT results on $YbFe_4Sb_{12}$ where avoided crossing was already reported [14–16]. An experimental proof of the avoided crossing found in DFT calculations has been provided in $LaFe_4Sb_4$ [16]. The avoided crossing is found in harmonic lattice dynamics calculations. Additionally, the Yb mode possesses the lowest frequency among the optical modes and is triply degenerated at the Γ point. It has the same Fu symmetry as the acoustic modes. This means that the acoustic modes can interact with this low optical energy mode (i.e., infrared-active) and the acoustic modes can hybridize with this low-energy optical mode and give the avoided crossing observed for many filled skutterudites [14–16].

To understand the interaction of the guest atom with the host lattice, we investigate the projected DOS of Sb and Yb atoms in $YbCo_4Sb_{12}$. As shown in Fig. 3(d), a rather sharp peak at 42 cm^{-1} is observed in the projected DOS of the Yb atom, corresponding to the flat guest mode in the phonon dispersions. Notice that there is some overlap between the Yb mode and Sb modes. The overlap region is from 30 to 150 cm^{-1}. Notably, a difference is found in the projected DOS of Sb atoms of $YbCo_4Sb_{12}$ and $CoSb_3$. This difference means that the Yb guest atom changes the DOS of the host atoms. These results suggest that the flat guest mode hybridizes with the host lattice.

E. Hybridization between the guest atom and host lattice

More evidence to support the hybridization of the guest atom and host lattice is needed. Figure 4(a) shows the lattice thermal conductivity for $YbCo_4Sb_{12}$ and $CoSb_3$ at 300 K from first-principles calculations. The total lattice thermal conductivity for $YbCo_4Sb_{12}$ and $CoSb_3$ at 300 K are listed in Table II. The previous experimental data and calculations are also listed for comparison. The lattice thermal conductivity for $CoSb_3$ at 300 K is slightly smaller than the experimental data and previous calculations [50,53–55]. The lattice thermal conductivity for $YbCo_4Sb_{12}$ at 300 K is comparable to the experimental data for $Yb_xCo_4Sb_{12}$ and $YbFe_4Sb_{12}$ [7,31,56–58], and slightly smaller than the calculations for $YbFe_4Sb_{12}$ [14].

For unfilled skutterudite $CoSb_3$, the contributions of the acoustic and optical modes to the lattice thermal conductivity are 77.6% and 22.4%, respectively. The lattice thermal conductivity is dominated by the acoustic modes. However, this is different in the case of $YbCo_4Sb_{12}$. The contributions of the acoustic modes, Yb mode, and optical modes in $YbCo_4Sb_{12}$ are 39.4%, 22.2%, and 38.4%, respectively. Notably, we find

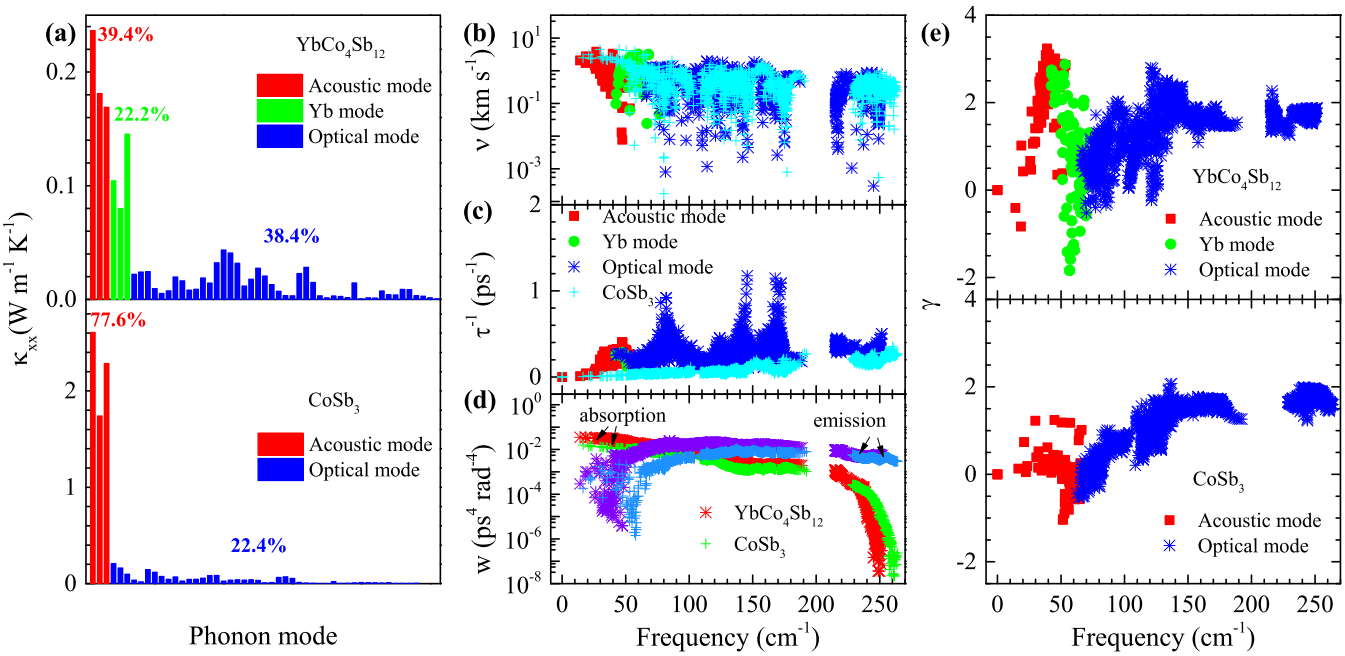

FIG. 4. Calculated κ (a), group velocities (v_m) (b), anharmonic scattering rates (τ^{-1}) (c), weighted phase space (w) (d), and mode-Grüneisen parameter (γ_i) (e) for $YbCo_4Sb_{12}$ and $CoSb_3$ at room temperature.

that the contribution of the optical modes is comparable to that of the acoustic mode and slightly higher than that of the Yb mode. In addition, the Yb mode also belongs to the optical modes. These findings imply that optical modes dominate the lattice thermal conductivity in $YbCo_4Sb_{12}$. Therefore filling Yb atoms affects the host lattice by increasing the relative contribution of the optical modes to the thermal conductivity and accordingly reducing that of the acoustic modes. Thus we believe that the hybridization occurs between the Yb atom and host lattice. This finding is also similar to the tight coupling between the guest atoms and the host lattice in (La, Ce)Fe_4Sb_{12} [12].

Understanding the effect of hybridization on lattice thermal conductivity requires taking into account group velocity and phonon lifetime. The lattice thermal conductivity can be estimated by the simple kinetic theory: $\kappa_l = 1/3\, C v_m \ell$, where C is the lattice specific heat, v_m is the mean sound velocity and ℓ is the mean free path of the phonons. From Dulong-Petit law, the specific heat increases with increasing temperature and gradually approaches a constant value above the Debye temperature which is here less than 300 K. Therefore the heat capacity does not influence the lattice thermal conductivity. According to the theory, the factors that might affect the lattice thermal conductivity are group velocity (v_m) and phonon lifetime (τ). Figure 4(b) shows the group velocities of $YbCo_4Sb_{12}$ and $CoSb_3$. For the acoustic modes and Yb mode, the group velocities of $YbCo_4Sb_{12}$ are much lower than those of $CoSb_3$. For the optical modes, the group velocities of $YbCo_4Sb_{12}$ and $CoSb_3$ are not much different. This means that the reduced group velocities within a narrow low-frequency range contribute to the suppressed lattice thermal conductivity in $YbCo_4Sb_{12}$.

TABLE II. Comparison of the lattice thermal conductivity κ_l (W K^{-1} m^{-1}) of $CoSb_3$, $Yb_xCo_4Sb_{12}$, and $YbFe_4Sb_{12}$.

	κ_l cal.	κ_l exp.
$CoSb_3$	8.55 (this work)	11.50 [54]
	11.67 [53]	10.00 [50]
		9.06 [55]
$YbCo_4Sb_{12}$	1.49 (this work)	
$Yb_xCo_4Sb_{12}$		1.60–2.00 (x = 0.25–0.40) [31]
		1.57–1.90 (x = 0.30–0.50) [56]
		1.68–2.27 (x = 0.30–0.40) [57]
		1.70–2.40 (x = 0.20–0.60) [7]
$YbFe_4Sb_{12}$	0.33 [14]	1.18 [58]

The phonon lifetime (τ) should be critical for the low lattice thermal conductivity in $YbCo_4Sb_{12}$. The scattering rate is the reverse of τ, defined by $\tau^{-1} = v_m/\iota$. To look into the effect of anharmonic interactions, we show the anharmonic scattering rates for $YbCo_4Sb_{12}$ and $CoSb_3$ in Fig. 4(c). The scattering rates of the optical modes are much larger than those of the acoustic modes. This means that the optical phonons also contribute significantly to the lattice thermal conductivity. The frequencies of the two peaks correspond to the phonon modes (F_g^3 at 149 cm^{-1} and E_g^2 at 182 cm^{-1}) as observed from the Raman spectra. The two phonon modes possess large Grüneisen parameters. Compared with $CoSb_3$, the anharmonic scattering rates of $YbCo_4Sb_{12}$ are apparently larger. These results imply that the large anharmonic scattering rates should be the main factor for the reduced lattice thermal conductivity in $YbCo_4Sb_{12}$.

The weighted phase space is a direct measure of the number of scattering processes available to each phonon [14]. The increased anharmonic scattering rates in filled skutterudites are related to the increased weighted phase space. As shown in Fig. 4(d), the weighted phase spaces of $YbCo_4Sb_{12}$ and $CoSb_3$ are similar in shape. These values for $YbCo_4Sb_{12}$ are much

TABLE III. Eigenfrequencies (in cm^{-1}) and mode-Grüneisen parameters of the Γ-point modes of $CoSb_3$ and $Yb_{0.3}Co_4Sb_{12}$ from the DFT calculations.

	$YbCo_4Sb_{12}$		$CoSb_3$	
symmetry	ω_i (cm^{-1})	γ_i	ω_i (cm^{-1})	γ_i
A_g	145.70	2.38	142.84	1.71
	167.75	1.75	170.36	1.68
E_g	124.03	2.66	127.35	1.67
	172.29	1.91	175.85	1.72
F_g	81.94	0.29	80.30	0.28
	98.79	1.03	103.79	0.94
	141.99	1.96	145.21	1.70
	171.03	1.53	174.32	1.47
A_u	102.60	0.34	108.52	0.21
	230.21	1.26	236.56	1.79
E_u	121.27	0.23	126.65	0.60
	247.59	1.52	249.59	1.97
Fu	42.50	2.74		
	84.37	1.23	75.74	0.02
	113.46	1.42	114.49	1.11
	135.52	2.24	137.56	1.52
	158.56	1.39	167.15	1.50
	216.04	1.81	231.08	1.68
	232.01	1.70	241.41	1.58
	249.29	1.82	256.99	1.77

larger than those of $CoSb_3$, indicating strong anharmonic scattering in $YbCo_4Sb_{12}$ due to the intercalation of Yb guest atoms.

F. Comparison of Grüneisen parameters between the experiments and calculations

To make the anharmonicity more quantitative, it would be valuable to gain the mode Grüneisen parameters of $YbCo_4Sb_{12}$ from first-principles calculations. For comparison, the data for $CoSb_3$ are also presented. As shown in the upper panel of Fig. 4(e), a strong peak for frequencies near the Yb mode can be found. The two peaks in the optical modes correspond to the two large mode Grüneisen parameters from our experiments. The Grüneisen parameters of the optical modes make a prominent contribution to the total Grüneisen parameter of $YbCo_4Sb_{12}$.

Compared with $CoSb_3$, the Grüneisen parameter of $YbCo_4Sb_{12}$ increases dramatically. The average Grüneisen parameters for $YbCo_4Sb_{12}$ and $CoSb_3$ are 1.48 and 1.19, respectively. The relatively large average Grüneisen parameter in $YbCo_4Sb_{12}$ indicates strong anharmonicity. This result agrees with our Raman scattering data.

The mode Grüneisen parameters of $YbCo_4Sb_{12}$ and $CoSb_3$ obtained from DFT calculations are given in Table III. Notably, the mode Grüneisen parameter of the Yb mode at 42 cm^{-1} is 2.74, which is the largest value among those of the other vibrational modes. Koza and coworkers [16] have reported the rather significant anharmonicity of the low-energy Yb mode compared to other MFe_4Sb_{12} (M = Ca, Sr, Ba) skutterudites through INS measurements and DFT calculations. Therefore $YbCo_4Sb_{12}$ has the proximity with $YbFe_4Sb_{12}$ and the anharmonicity of Yb mode is important. The mode Grüneisen parameter of the Yb mode at 42 cm^{-1} is also slightly larger than that of Eu mode at 56 cm^{-1} (γ = 2.5) in $Eu_{0.84}Fe_4Sb_{12}$ found from x-ray powder diffraction and nuclear inelastic scattering experiments under pressure [46]. The strong anharmonicity accounts for the low lattice thermal conductivity in $YbCo_4Sb_{12}$.

The above observations also reveal the importance of the optical phonon modes in the lattice thermal conductivity of filled skutterudites. Unlike $CoSb_3$, the optical phonon modes in $YbCo_4Sb_{12}$ play a dominant role in both the lattice thermal conductivity and Grüneisen parameters. Therefore investigating the optical phonon modes is very important. The phonon modes observed in the Raman spectra should be particularly important. The frequencies corresponding to large mode Grüneisen parameters for $Yb_{0.3}Co_4Sb_{12}$ are observed in our Raman scattering measurements. The values of the Grüneisen parameters of $Yb_{0.3}Co_4Sb_{12}$ are slightly larger than those of $CoSb_3$. The low Grüneisen parameter value for the F_g^1 mode at about 82 cm^{-1} is very close to the one predicted for $CoSb_3$ by DFT calculations [47].

Combining the results from experiments and calculations, we provide an understanding of the low lattice thermal conductivity for $Yb_{0.3}Co_4Sb_{12}$. We find that the strong anharmonicity reduces the lattice thermal conductivity in the sample. The depressed group velocity within the low-frequency range and the flat guest mode avoided crossing with the acoustic-phonon mode also contributes to the suppression of the lattice thermal conductivity. The optical phonons are important for lowering the lattice thermal conductivity. Our results suggest that the reduction effect of the guest atom on the lattice thermal conductivity is not the same as the PGEC theory or the case in filled Fe_4Sb_{12}-type skutterudites [10,12]. The guest atom hybridizes with the host lattice rather than acting as scattering centers. This gives unequivocal evidence that the second Einstein mode observed in $Yb_{0.3}Co_4Sb_{12}$ [13] is due to the hybridization of the guest atom and cage lattice. The DFT calculations indicate that both the hybridization of acoustic and optical modes seen in the harmonic calculations and the enhanced anharmonicity linked to that and observed in the anharmonic calculations can explain the reduction of the thermal conductivity in filled skutterudites compared with $CoSb_3$.

IV. CONCLUSIONS

In summary, by combining high-pressure x-ray diffraction and Raman scattering measurements as well as first-principles calculations, we have investigated the structural and thermal transport properties of $Yb_{0.3}Co_4Sb_{12}$. The phase transition in the sample is found to occur at pressure of around 12.4 GPa. The bulk modulus at ambient pressure has been determined through the volume evolution with pressure. Based on the bulk modulus and the phonon frequency shifts, we have obtained the mode Grüneisen parameter for each observed phonon mode. Compared with the unfilled parent, the obtained relatively large Grüneisen parameters in the studied material indicate that the low lattice thermal conductivity is attributed to the strong anharmonicity. In addition, the depressed group velocity within the low-frequency range and the flat guest mode avoided crossing with the acoustic-phonon mode also contribute to the lattice thermal conductivity reduction. Optical phonon modes were found to be important for lowing

the lattice thermal conductivity of $Yb_{0.3}Co_4Sb_{12}$. Compared with $CoSb_3$, the low lattice thermal conductivity for filled skutterudites is mainly due to the hybridization between the guest atom and host lattice and the associated enhanced anharmonicity. These findings provide novel insights for understanding the mechanism behind the low lattice thermal conductivity in filled skutterudites.

ACKNOWLEDGMENTS

We thank X. Shi and L. D. Chen for providing samples and valuable discussions. We are grateful for the helpful guidance from Xiao-Qun Wang from Shanghai Jiaotong University. This work is funded through the National Key R&D Program of China (Grant No. 2018YFA0305900) at HPSTAR, the Shenzhen Science and Technology Program (Grant No. KQTD20200820113045081), and the Basic Research Program of Shenzhen (Grant No. JCYJ20200109112810241) at HIT. The research used resources of the Advanced Photon Source, a U.S. Department of Energy (DOE) Office of Science User Facility operated for the DOE Office of Science by Argonne National Laboratory under Contract No. DE-AC02-06CH11357.

[1] G. J. Snyder and E. S. Toberer, Complex thermoelectric materials, Nat. Mater. **7**, 105 (2008).

[2] B. Poudel, Q. Hao, Y. Ma, Y. C. Lan, A. Minnich, B. Yu, X. Yan, D. Z. Wang, A. Muto, D. Vashaee, X. Y. Chen, J. M. Liu, M. S. Dresselhaus, G. Chen, and Z. F. Ren, High-thermoelectric performance of nanostructured bismuth antimony telluride bulk alloys, Science **320**, 634 (2008).

[3] K. Biswas, J. Q. He, I. D. Blum, C. I. Wu, T. P. Hogan, D. N. Seidman, V. P. Dravid, and M. G. Kanatzidis, High-performance bulk thermoelectrics with all-scale hierarchical architectures, Nature (London) **489**, 414 (2012).

[4] J. Ma, O. Delaire, A. F. May, C. E. Carlton, M. A. McGuire, L. H. VanBebber, D. L. Abernathy, G. Ehlers, T. Hong, A. Huq, W. Tian, V. M. Keppens, Y. Shao-Horn, and B. C. Sales, Glass-like phonon scattering from a spontaneous nanostructure in $AgSbTe_2$, Nat. Nanotechnol. **8**, 445 (2013).

[5] G. P. Meisner, D. T. Morelli, S. Hu, J. Yang, and C. Uher, Structure and Lattice Thermal Conductivity of Fractionally Filled Skutterudites: Solid Solutions of Fully Filled and Unfilled End Members, Phys. Rev. Lett. **80**, 3551 (1998).

[6] T. Dahal, Q. Jie, G. Joshi, S. Chen, C. F. Guo, Y. C. Lan, and Z. F. Ren, Thermoelectric property enhancement in Yb-doped *n*-type skutterudites $Yb_xCo_4Sb_{12}$, Acta Mater. **75**, 316 (2014).

[7] S. Y. Wang, J. R. Salvador, J. Yang, P. Wei, B. Duan, and J. H. Yang, High-performance *n*-type $Yb_xCo_4Sb_{12}$: From partially filled skutterudites towards composite thermoelectrics, NPG Asia Mater **8**, e285 (2016).

[8] X. Shi, S. Q. Bai, L. L. Xi, J. Yang, W. Q. Zhang, L. D. Chen, and J. H. Yang, Realization of high thermoelectric performance in *n*-type partially filled skutterudites, J. Mater. Res. **26**, 1745 (2011).

[9] X. Shi, J. Yang, J. R. Salvador, M. F. Chi, J. Y. Cho, H. Wang, S. Q. Bai, J. H. Yang, W. Q. Zhang, and L. D. Chen, Multiple-filled Skutterudites: High thermoelectric figure of merit through separately optimizing electrical and thermal transports, J. Am. Chem. Soc. **133**, 7837 (2011).

[10] G. A. Slack, in CRC handbook of thermoelectrics, edited by D. M. Rowe (CRC, Boca Raton, FL, 1995).

[11] G. S. Nolas, D. T. Morelli, and T. M. Tritt, Skutterudites: A phonon-glass-electron-crystal approach to advanced thermoelectric energy conversion applications, Annu. Rev. Mater. Sci. **29**, 89 (1999).

[12] M. M. Koza, M. R. Johnson, R. Viennois, H. Mutka, L. Girard, and D. Ravot, Breakdown of phonon glass paradigm in La- and Ce-filled Fe_4Sb_{12} skutterudites, Nat. Mater. **7**, 805 (2008).

[13] I. K. Dimitrov, M. E. Manley, S. M. Shapiro, J. Yang, W. Zhang, L. D. Chen, Q. Jie, G. Ehlers, A. Podlesnyak, J. Camacho, and Q. Li, Einstein modes in the phonon density of states of the single-filled skutterudite $Yb_{0.2}Co_4Sb_{12}$, Phys. Rev. B **82**, 174301 (2010).

[14] W. Li and N. Mingo, Ultralow lattice thermal conductivity of the fully filled skutterudite $YbFe_4Sb_{12}$ due to the flat avoided-crossing filler modes, Phys. Rev. B **91**, 144304 (2015).

[15] M. M. Koza, M. Boehm, E. Sischka, W. Schnelle, H. Mutka, and A. Leithe-Jasper, Low-energy phonon dispersion in $LaFe_4Sb_{12}$, Phys. Rev. B **91**, 014305 (2015).

[16] M. M. Koza, A. Leithe-Jasper, H. Rosner, W. Schnelle, H. Mutka, M. R. Johnson, M. Krisch, L. Capogna, and Y. Grin, Vibrational dynamics of the filled skutterudites $M_{1-x}Fe_4Sb_{12}$ (M = Ca, Sr, Ba, and Yb): Temperature response, dispersion relation, and material properties, Phys. Rev. B **84**, 014306 (2011).

[17] C. Chang and L. D. Zhao, Anharmoncity and low thermal conductivity in thermoelectrics, Mater. Today Phys. **4**, 50 (2018).

[18] V. Keppens, D. Mandrus, B. C. Sales, B. C. Chakoumakos, P. Dai, R. Coldea, M. B. Maple, D. A. Gajewski, E. J. Freeman, and S. Bennington, Localized vibrational modes in metallic solids, Nature (London) **395**, 876 (1998).

[19] X. J. Chen, V. V. Struzhkin, S. Kung, H. K. Mao, R. J. Hemley, and A. N. Christensen, Pressure-induced phonon frequency shifts in transition-metal nitrides, Phys. Rev. B **70**, 014501 (2004).

[20] M. Christensen, A. B. Abrahamsen, N. B. Christensen, F. Juranyi, N. H. Andersen, K. Lefmann, J. Andreasson, C. R. H. Bahl, and B. B. Iversen, Avoided crossing of rattler modes in thermoelectric materials, Nat. Mater. **7**, 811 (2008).

[21] C. W. Li, J. Hong, A. F. May, D. Bansal, S. Chi, T. Hong, G. Ehlers, and O. Delaire, Orbitally driven giant phonon anharmonicity in SnSe, Nat. Phys. **11**, 1063 (2015).

[22] L. C. Chen, Z. Y. Cao, H. Yu, B. B. Jiang, L. Su, X. Shi, L. D. Chen, and X. J. Chen, Phonon anharmonicity in thermoelectric palladium sulfide by Raman spectroscopy, Appl. Phys. Lett. **113**, 022105 (2018).

[23] Z. Y. Cao and X. J. Chen, Phonon scattering processes in molybdenum disulfide, Appl. Phys. Lett. **114**, 052102 (2019).

[24] H. J. Pang, L. C. Chen, Z. Y. Cao, H. Yu, C. G. Fu, T. J. Zhu, A. F. Goncharov, and X. J. Chen, Mode Grüneisen parameters of an efficient thermoelectric half-Heusler, J. Appl. Phys. **124**, 195107 (2018).

[25] L. C. Chen, Q. Peng, H. Yu, H. J. Pang, B. B. Jiang, L. Su, X. Shi, L. D. Chen, and X. J. Chen, Lattice dynamics of thermoelectric palladium sulfide, J. Alloys Compd. **798**, 484 (2019).

[26] H. Yu, G. Huang, Q. Peng, L. C. Chen, H. J. Pang, X. Y. Qin, P. F. Qiu, X. Shi, L. D. Chen, and X. J. Chen, A combined experiment and first-principles study on lattice dynamics of thermoelectric $CuInTe_2$, J. Alloys Compd. **822**, 153610 (2020).

[27] Y. Zhou, Z. Y. Dong, W. P. Hsieh, A. F. Goncharov, and X. J. Chen, Thermal conductivity of materials under pressure, Nat. Rev. Phys. (2022).

[28] G. S. Nolas and G. A. Slack, Raman scattering study of antimony based skutterudites, J. Appl. Phys. **79**, 2622 (1996).

[29] G. S. Nolas and C. A. Kendziora, Raman spectroscopy investigation of lanthanide-filled and unfilled skutterudites, Phys. Rev. B **59**, 6189 (1999).

[30] L. X. Li, H. Liu, J. Y. Wang, X. B. Hu, S. R. Zhao, H. D. Jiang, Q. J. Huang, H. H. Wang, and Z. F. Li, Raman spectroscopy investigation of partially filled skutterudite, Chem. Phys. Lett. **347**, 373 (2001).

[31] Y. L. Li, P. F. Qiu, Z. Xiong, J. K. Chen, R. Nunna, X. Shi, and L. D. Chen, Electrical and thermal transport properties of $Yb_xCo_4Sb_{12}$ filled skutterudites with ultrahigh carrier concentrations, AIP Adv. **5**, 117239 (2015).

[32] H. K. Mao, P. M. Bell, J. W. Shaner, and D. J. Stembey, Specific volume measurements of Cu, Mo, Pd, and Ag and calibration of the ruby R1 fluorescence pressure gauge from 0.06 to 1 Mbar, J. Appl. Phys. **49**, 3276 (1978).

[33] A. P. Hammersley, S. O. Svensson, M. Hanfland, A. N. Fitch, and D. Hausermann, Two-dimensional detector software: From real detector to idealised image or two-theta scan, High Press. Res. **14**, 235 (1996).

[34] A. C. Larson and R. B. Von Dreele, GSAS (general structure analysis system), Los Alamos National Laboratory Report LAUR, 86 (1994).

[35] B. H. Toby, EXPGUI, a graphical user interface for GSAS, J. Appl. Crystallogr. **34**, 210 (2001).

[36] G. Kresse and J. Joubert, From ultrasoft pseudopotentials to the projector augmented-wave method, Phys. Rev. B **59**, 1758 (1999).

[37] G. Kresse and J. Furthmüller, Efficient iterative schemes for *ab initio* total-energy calculations using a plane-wave basis set, Phys. Rev. B **54**, 11169 (1996).

[38] J. P. Perdew, K. Burke, and M. Ernzerhof, Generalized Gradient Approximation Made Simple, Phys. Rev. Lett. **77**, 3865 (1996).

[39] A. Togo, F. Oba, and I. Tanaka, First-principles calculations of the ferroelastic transition between rutile-type and $CaCl_2$-type SiO_2 at high pressures, Phys. Rev. B **78**, 134106 (2008).

[40] W. Li, J. Carrete, N. A. Katcho, and N. Mingo, ShengBTE: a solver of the Boltzmann transport equation for phonons, Comput. Phys. Commun. **185**, 1747 (2014).

[41] W. F. Sherman, Bond anharmonicities, Grüneisen parameters and pressure-induced frequency shifts, J. Phys. C: Solid State Phys. **13**, 4601 (1980).

[42] F. D. Murnaghan, The compressibility of media under extreme pressure, Proc. Natl. Acad. Sci. U.S.A. **30**, 244 (1944).

[43] A. C. Kraemer, M. R. Gallas, J. A. H. da Jornada, and C. A. Perottoni, Pressure-induced self-insertion reaction in $CoSb_3$, Phys. Rev. B **75**, 024105 (2007).

[44] A. C. Kraemer, C. A. Perottoni, and J. A. H. D. Jornada, Isothermal equation of state for skutterudites $CoSb_3$ and $LaFe_3CoSb_{12}$, Solid State Commun. **133**, 173 (2005).

[45] W. Liu, Q. Jie, Q. Li, Z. Q. Chen, and B. S. Li, Synchrotron X-ray study of filled skutterudites $CeFe_4Sb_{12}$ and $Ce_{0.8}Fe_3CoSb_{12}$, Phys. B: Condens. Matter **406**, 52 (2011).

[46] I. Sergueev, K. Glazyrin, I. Kantor, M. A. McGuire, A. I. Chumakov, B. Klobes, B. C. Sales, and R. P. Hermann, Quenching rattling modes in skutterudites with pressure, Phys. Rev. B **91**, 224304 (2015).

[47] R. Viennois, T. Kume, M. Komura, L. Girard, A. Haidoux, J. Rouquette, and M. M. Koza, Raman-scattering experiments on unfilled skutterudite $CoSb_3$ under high pressure and high temperature, J. Phys. Chem. C **124**, 23004 (2020).

[48] G. S. Nolas, C. A. Kendziora, and Hirotsugu Takizawa, Polarized Raman-scattering study of Ge and Sn-filled $CoSb_3$, J. Appl. Phys. **94**, 7440 (2003).

[49] I. Shirotani, T. Noro, J. Hayashi, C. Sekine, R. Giri, and K. Kikegawa, X-ray study with synchrotron radiation for P- and Sb-based skutterudite compounds at high pressures, J. Phys.: Condens. Matter **16**, 7853 (2004).

[50] T. Caillat, A. Borshchevsky, and J. P. Fleuril, Properties of single crystalline semiconducting $CoSb_3$, J. Appl. Phys. **80**, 4442 (1996).

[51] J. L. Feldman and D. J. Singh, Lattice dynamics of skutterudites: First-principles and model calculations for $CoSb_3$, Phys. Rev. B **53**, 6273 (1996).

[52] J. Yang, W. Zhang, S. Q. Bai, Z. Mei, and L. D. Chen, Dual-frequency resonant phonon scattering in $Ba_xR_yCo_4Sb_{12}$ (R = La, Ce, and Sr), Appl. Phys. Lett. **90**, 192111 (2007).

[53] W. Li and N. Mingo, Lattice dynamics and thermal conductivity of skutterudites $CoSb_3$ and $IrSb_3$ from first principles: Why $IrSb_3$ is a better thermal conductor than $CoSb_3$, Phys. Rev. B **90**, 094302 (2014).

[54] D. T. Morelli, T. Caillat, J.-P. Fleurial, A. Borshchevsky, J. Vandersande, B. Chen, and C. Uher, Low-temperature transport properties of *p*-type $CoSb_3$, Phys. Rev. B **51**, 9622 (1995).

[55] B. C. Sales, D. Mandrus, B. C. Chakoumakos, V. Keppens, and J. R. Thompson, Filled skutterudite antimonides: Electron crystals and phonon glasses, Phys. Rev. B **56**, 15081 (1997).

[56] J. Yang, Q. Hao, H. Wang, Y. C. Lan, Q. Y. He, A. Minnich, D. Z. Wang, J. A. Harriman, V. M. Varki, M. S. Dresselhaus, G. Chen, and Z. F. Ren, Solubility study of Yb in *n*-type skutterudites $Yb_xCo_4Sb_{12}$ and their enhanced thermoelectric properties, Phys. Rev. B **80**, 115329 (2009).

[57] Y. L. Tang, S. W. Chen, and G. J. Snyder, Temperature dependent solubility of Yb in Yb-$CoSb_3$ skutterudite and its effect on preparation, optimization and lifetime of thermoelectrics, Journal of Materiomics **1**, 75 (2015).

[58] P. F. Qiu, J. Yang, R. H. Liu, X. Shi, X. Y. Huang, G. J. Snyder, W. Zhang, and L. D. Chen, High-temperature electrical and thermal transport properties of fully filled skutterudites RFe_4Sb_{12} (R=Ca, Sr, Ba, La, Ce, Pr, Nd, Eu, and Yb), J. Appl. Phys. **109**, 063713 (2011).